AGU PUBLICATIONS

Geochemistry, Geophysics, Geosystems

RESEARCH ARTICLE
10.1002/2016GC006248

Key Points:
- The Early cretaceous intermediate magmatic rocks were derived by partial melting of melange diapir
- The Early cretaceous intermediate rocks have an overall continental crust-like andesitic composition
- Melange melting provides a support for the "andesite model" for continental crustal growth

Supporting Information:
- Supporting Information S1

Correspondence to:
Q. Wang,
wqiang@gig.ac.cn

Citation:
Hao, L.-L., Q. Wang, D. A. Wyman, Q. Ou, W. Dan, Z.-Q. Jiang, J.-H. Yang, J. Li, and X.-P. Long (2016), Andesitic crustal growth via mélange partial melting: Evidence from Early Cretaceous arc dioritic/andesitic rocks in southern Qiangtang, central Tibet, *Geochem. Geophys. Geosyst.*, *17*, 1641–1659, doi:10.1002/2016GC006248.

Received 7 JAN 2016
Accepted 6 APR 2016
Accepted article online 6 MAY 2016

Andesitic crustal growth via mélange partial melting: Evidence from Early Cretaceous arc dioritic/andesitic rocks in southern Qiangtang, central Tibet

Lu-Lu Hao[1,2], Qiang Wang[1,3], Derek A. Wyman[4], Quan Ou[1,2], Wei Dan[1], Zi-Qi Jiang[1,5], Jin-Hui Yang[6], Jie Li[1], and Xiao-Ping Long[1]

[1]State Key Laboratory of Isotope Geochemistry, Guangzhou Institute of Geochemistry, Chinese Academy of Sciences, Guangzhou, China, [2]University of Chinese Academy of Sciences, Beijing, China, [3]CAS Center for Excellence in Tibetan Plateau Earth Sciences, Beijing, China, [4]School of Geosciences, University of Sydney, New South Wales, Australia, [5]School of Earth Science, Guilin University of Technology, Guilin, China, [6]Institute of Geology and Geophysics, Chinese Academy of Science, Beijing, China

Abstract Deciphering the petrogenesis of andesitic/dioritic rocks is fundamental to understanding the formation of the continental crust. Here we present detailed petrology, geochronology, major and trace element, Sr–Nd–Hf–O isotope data for the Early Cretaceous (~122 Ma) dioritic rocks in the Bizha area in southern Qiangtang, Tibet. The dioritic rocks are characterized by large ion lithophile elements, Pb, and light rare earth elements but depletion of high field strength elements with slightly enriched and variable εNd(t) values of −0.01 to −3.31 and initial $^{87}Sr/^{86}Sr$ isotopic ratios of 0.7053–0.7062. They also have variable magmatic zircon Hf-O isotope compositions (εHf(t) = −5.3 to +3.6 and $\delta^{18}O$ = +7.3 to +9.5 ‰). Combined with contemporary andesitic lavas in southern Qiangtang, we suggest that the intermediate magmatic rocks in this area were most probably derived by partial melting of a subduction mélange, which is a mixture of mid-oceanic ridge basalts (MORBs), sediments, and mantle wedge peridotites, formed along the interface between the subducted slab and the overlying mantle wedge in a subduction channel before ~124 Ma. The mélange diapir melting was triggered by the asthenospheric upwelling and hot corner flow caused by roll-back of the northward subducted Bangong-Nujiang oceanic slab during the Early Cretaceous. The Early Cretaceous intermediate magmatic rocks in southern Qiangtang have an overall continental crust-like andesitic composition. Therefore, partial melting of mélange provides an important support for the generation of andesitic magmas in continental arcs and the "andesite model" for crustal growth.

1. Introduction

One of the Earth's unique features when compared with other rocky planets in our Solar System is the presence of continental crust [*Rudnick*, 1995]. There is, however, considerable debate regarding when and how the crust formed, especially the processes responsible for its evolved composition [*Rudnick*, 1995]. The Earth's continents are mostly composed of igneous and metaigneous rocks that on average yield an andesite composition with SiO_2 = 60.6 wt. % and MgO = 4.7 wt. % [*Taylor and McLennan*, 1985; *Rudnick and Gao*, 2003], or a more felsic composition with SiO_2 = 65.2 wt. % and MgO = 2.5 wt. % [*Hacker et al*., 2011]. However, the continental crust as a whole is believed to be ultimately derived from the underlying mantle and thus should have a basaltic composition complementary to the Earth's mantle [*Hofmann*, 1988]. Thus, the difference in compositions between mantle-derived basaltic melts and the bulk andesitic continental crust leads to an intriguing paradox in Earth Science [e.g., *Castro et al*., 2013].

Hypotheses to account for this paradox can be grouped in two categories [e.g., *Castro et al*., 2013]. One is a basalt-input model and the other is a primary andesite model. The basalt-input model postulates that the composition of magma fluxing the continental crust is basaltic, which is derived from the peridotite mantle. In this scenario, andesitic rocks are generated by magma mixing or AFC (assimilation fractional crystallization) processes acting on primitive basaltic magma in the deep crust of continental arcs [e.g., *Hildreth and Moorbath*, 1988]. The elimination of a hypothetical ultramafic residue by sinking into the underlying mantle is then required to counterbalance the andesitic compositions of the bulk continental crust [*Rudnick*, 1995].

Recently, however, *Castro et al*. [2013] suggested that this classic model failed to account for two fundamental facts: the absence of ultramafic residues in the lower crust and the high temperature of batholith magma generation. In addition, *Zheng et al*. [2015] proposed that a corresponding occurrence of abundant basalts and gabbros is required to validate this model, with quantitative consideration of volume proportions between the mafic and felsic rocks; otherwise it remains only a hypothesis. The other group of hypotheses is represented by the andesite model formulated by *Taylor* [1967]. In this model, arcs directly produce andesitic magmas, in accord with the broadly andesitic bulk composition of the continental crust and slab-mantle reaction is presumably regarded as a vital step to generate the andesitic rocks [e.g., *Kelemen*, 1995; *Zheng*, 2012]. Considering that oceanic arcs are dominated by basalts whereas continental arcs are dominated by andesites, the preferred occurrence of andesites in a continental arc may be related to the larger amounts of the sediment subducted into mantle in a continental arc compared to an oceanic arc [e.g., *Chen et al*., 2014; *Zhao et al*., 2013; *Zheng et al*., 2015]. In an Andes-type subduction zone, large amounts of sediment can easily be subducted into mantle by subduction erosion [e.g., *von Huene and Scholl*, 1991].

Two main versions of the slab-mantle reaction model have been proposed [e.g., *Castro et al*., 2010, 2013; *Kelemen*, 1995; *Zheng*, 2012]. The first hypothesizes that due to more felsic components being incorporated into the mantle beneath continental arcs, the metasomatized mantle source of andesitic magmas becomes less ultramafic than the mantle source of oceanic arc basalts. Partial melting of the less ultramafic metasomatites then yields andesitic melts [*Zheng*, 2012]. The alternative version, based on the results of recent numerical and laboratory experiments, suggests that melts of subducted oceanic crust and sediments react with the mantle to produce andesite magmas that are directly responsible for the generation of new continental crust [*Castro et al*., 2010, 2013]. The andesitic magmas are ultimately added to the continental crust where they partially crystallize and separate into a solid fraction to form lower crust mafic granulite and granitic liquids to form upper crust batholiths [*Castro et al*., 2013]. Thus, the specific physical mechanism for mixing and transport of slab materials and mantle wedge has been enigmatic. Recently, *Marschall and Schumacher* [2012], based on numerical thermomechanical modeling [*Gerya and Yuen*, 2003; *Gerya et al*., 2004] and experimental phase relations [*Castro et al*., 2010], proposed that arc magmas are probably sourced from mélange diapirs in subduction zones. The mélange is a mixture of MORB, sediments and mantle wedge and forms along the interface between the subducted slab and the mantle in a subduction channel [*Marschall and Schumacher*, 2012]. It may well provide a mechanism for slab-mantle mixing and reaction. However, this conceptual model of mélange partial melting requires further validation, given that it would likely be fundamental to understanding the formation of andesitic continental crust.

In southern Qiangtang, central Tibet, Late Mesozoic intermediate-felsic magmatic rocks are far more abundant than basic rocks. *Hao et al*. [2016] tracked the sources of late-Mesozoic felsic rocks in southern Qiangtang (between the Bangong Co and Dongqiao areas) and suggested that vertical crustal growth occurred in the area by magma underplating in a continental arc setting. The nature of the underplated magmas, however, remains unknown. In this study, we focus on studying the intermediate rocks in southern Qiangtang for a better understanding of the petrogenesis of andesitic rocks and its connection with crustal growth. We present detailed petrology, geochronology, whole-rock major and trace element, Sr–Nd and zircon Hf–O isotopic data for the Early Cretaceous dioritic pluton in the Bizha area in order to delineate the petrogenesis of the dioritic rocks. Together with previous studies of the andesitic lavas in southern Qiangtang, these data contribute to a better understanding of continental crust growth and the evolution of continental arcs.

2. Geological Setting and Rock Characteristics

The Tibetan plateau comprises the Qaidam, Songpan-Ganze-Hoh Xil, Qiangtang, Lhasa, and Himalaya blocks from north to south. These blocks are separated by four sutures (Anyimaqin-Kunlun-Muztagh, Jinsha, Bangong-Nujiang, and Indus-Yalu Sutures, respectively) (Figure 1a) [*Chung et al*., 2005; *Yin and Harrison*, 2000]. The Qiangtang block is located in central Tibet, bounded by the Jinsha Suture (JS) to the north and the Bangong-Nujiang Suture (BNS) to the south (Figure 1a) [*Yin and Harrison*, 2000]. It can be divided into southern and northern Qiangtang separated by Longmu-Shuanghu Suture (Figure 1a) [*Li et al*., 2006]. The southern Qiangtang is located between the Longmu-Shuanghu and Bangong-Nujiang Sutures (Figure 1b). The exposed Amdo Neoproterozoic-Early Paleozoic basement orthogneisses in southern Qiangtang may represent an isolated microcontinent (Figure 1b), which collided with southern Qiangtang during the

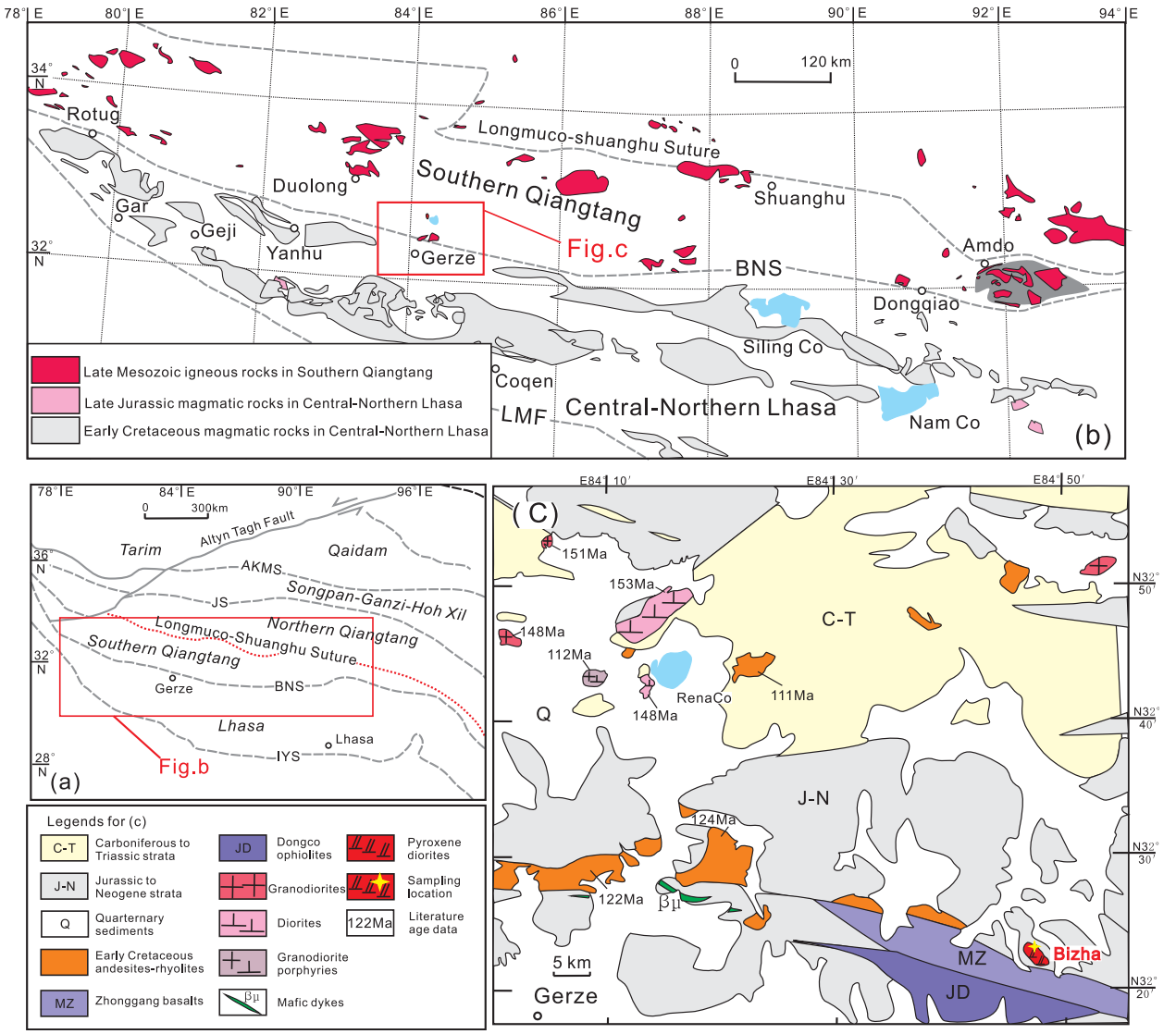

Figure 1. (a) Tectonic framework of the Tibetan Plateau (modified from diagrams of *Chung et al.* [2005] and *Yin and Harrison* [2000]. Main suture zones between major blocks: AKMS, Ayimaqen-Kunlun-Mutztagh suture; JS, Jinsha suture; BNS, Bangong-Nujiang suture; IYS, Indus-Yalu suture. (b) Map of the central Tibetan Plateau showing the distribution of Late Mesozoic igneous rocks in southern Qiangtang and central-northern Lhasa. LMF, Luobadui-Milanshan Fault. (c) Geological map of the studied area near the Gerze County. The Dongco ophiolite in the Gerze area is a part of the BNS. The literature age data are from: *Chang et al.* [2011]; *Hao et al.* [2016]; *Kapp et al.* [2005]; and *S. Liu et al.* [2012].

middle Jurassic (190–170 Ma) [e.g., *Guynn et al.*, 2006]. The collision is considered to have resulted in the deep subduction of this microcontinent beneath southern Qiangtang, the high-grade metamorphism (amphibolite and granulite facies) of the Amdo basement and the Early Jurassic magmatism (190–170 Ma) in the Amdo microcontinent [e.g., *Guynn et al.*, 2013; *X. R. Zhang et al.*, 2014].

The Bangong-Nujiang Suture Zone (BNSZ), which extends over 2000 km across central Tibet (Figure 1b), is characterized by mainly Jurassic-Cretaceous flysch, mélange, and scattered ophiolitic fragments and could represent remnants of the Bangong-Nujiang ocean basin [*Kapp et al.*, 2003]. The main strata exposed in southern Qiangtang consist of Carboniferous and Permian interbedded sandstone, shale and limestone, Permian interbedded sandstone, slate and limestone, and Jurassic sandstone and limestone, all of which have been intruded by Jurassic and Cretaceous intrusions [*Kapp et al.*, 2003]. Volcanic rocks occur in the Longge, Riganpeico, Mugagangri, Quse, Sewa, Meiriqieco, and Abushan groups [*Zhu et al.*, 2016]. Existing studies indicated that a period of intense magmatism occurred in southern Qiangtang and spanned the Bangong Co area in the west, the central Duolong and Gerze areas, and the Dongqiao and Amdo areas in the east [e.g., *Zhu et al.*, 2016]. These magmatic rocks (Figure 1b) are dominated by intermediate-felsic rocks,

and were emplaced between 170 and 101 Ma [e.g., *Chang et al*., 2011; *Kapp et al*., 2005; *J. X. Li et al*., 2011, 2013, 2014; *S.-M. Li et al*., 2014; *D. Liu et al*., 2014, 2015; *S. Liu et al*., 2012)].

In the Bangong Co area, the Larelaxin and Caima quartz diorites and biotite monzogranites plutons yielded zircon U-Pb ages of 168–160 Ma [*S.-M. Li et al*., 2014; *D. Liu et al*., 2014]. In addition, the adakitic Rutog granites were emplaced at 101 Ma [*D. Liu et al*., 2014].

In the Duolong Cu-Au deposit and surrounding areas, ore-bearing granodiorite porphyries were emplaced at 117 Ma [e.g., *Li et al*., 2013]. Premineralization basalts, synmineralization basaltic andesites, and post mineralization andesites were generated in 142, 118, and 106 Ma, respectively [e.g., *Li et al*., 2013]. Bimodal volcanic rocks (basalts and dacites) from the Maierze Group with ages of ~122 Ma [*Fan et al*., 2015], and voluminous intermediate-felsic plutons with ages of 170–115 Ma occur in the Qingcaoshan and Liqunshan areas, northwest of the Duolong Cu-Au deposit [*J. X. Li et al*., 2014; *Zhu et al*., 2016].

In the Gerze area, the Rena Co plutons mainly consists of Late Jurassic (~150 Ma) granodiorites and diorites and Early Cretaceous (~112 Ma) granodiorite porphyries [*Hao et al*., 2016]. Andesites and rhyolites in the area have been dated between 124 and 105 Ma [e.g., *Kapp et al*., 2005; *S. Liu et al*., 2012].

In the Dongqiao area, the Kangri pluton located to the northwest of Zugetang Co consists primarily of granodiorites and granites. Recent zircon U-Pb dating of the pluton yielded ages of 117–102 Ma [*D. Liu et al*., 2015]. Slightly further east in the Amdo area (Figure 1b), Late Jurassic volcanic rocks (mainly andesites) and Early Cretaceous (~122–112 Ma) granitic plutons were reported [*D. Liu et al*., 2015].

The recently discovered giant Cretaceous Duolong porphyry Cu-Au deposit (5.4 Mt at 0.72% Cu, 41 t at 0.23 g/t Au) in the Duolong-Gerze area (Figure 1b) is one of the largest known deposits in Tibet, China [e.g., *Qu and Xin*, 2006; *Li et al*., 2013]. Molybdenite Re-Os dating indicates an ore formation age of ~118 Ma [*She et al*., 2009]. This discovery provides significant additional motivation to better understand the petrogenesis of the Early Cretaceous magmatic rocks and geodynamic process in this area.

The Bizha pluton investigated in this study occurs to the east of Gerze County (Figure 1c). It primarily consists of gabbroic diorites and pyroxene diorites. These rocks are generally fresh without visible alteration and are medium to coarse-grained rocks, mainly consisting of plagioclase, biotite, amphibole, and clinopyroxene with minor orthopyroxene and alkali feldspar (see Supporting Information). Accessory phases include Fe-Ti oxides, apatite, zircon, and sphene.

3. Results

Analytical methods, photomicrographs, diagrams of mineral composition, and mineral composition, whole-rock major and trace elements and Sr-Nd isotope, LA-ICPMS zircon U-Pb and Hf isotope, and SIMS zircon O isotope data for the Bizha intrusive rocks are given in Supporting Information, respectively. We selected the least altered samples for geochemical and isotopic analyses.

3.1. Zircon U–Pb Dating Results

The LA-ICPMS zircon U–Pb isotope data for the Bizha pluton are illustrated in Figure 2. Most of the zircon grains are granular or platy with variable grain sizes of 50–200 m and length to width ratios of 1:1–3:1 (Figure 2). The oscillatory zoning cathodoluminescence images and high Th/U ratios (0.3–1.5) suggest magmatic origins [*Belousova et al*., 2002]. These zircon grains have a wide range of U (70–1007 ppm) and Th (55–700 ppm) concentrations. Twenty zircon U–Pb analyses for gabbroic diorite sample ZB140-2 are concordant and yield a weighted mean $^{206}Pb/^{238}U$ age of 121.3 ± 0.9 Ma (MSWD = 0.98). Three pyroxene diorite samples ZB140-1, ZB141-1, and ZB142-3 give weighted mean $^{206}Pb/^{238}U$ ages of 122.9 ± 1.9, 122.2 ± 1.8, and 121.8 ± 1.7 Ma, respectively. No old inherited zircons were found among analyzed zircon grains for four samples of the Bizha dioritic pluton. Therefore, this pluton was generated in the Early Cretaceous (~122 Ma), similar to the Duolong synmineralization basaltic andesites (~118 Ma) [*Li et al*., 2013] and the northern Gerze andesites (~124 Ma) [*S. Liu et al*., 2012].

3.2. Mineral Compositions

Clinopyroxenes in the Bizha pluton are salites or augites and orthopyroxenes are hypersthenes that are often surrounded by clinopyroxenes. The hypersthene grains have high MgO (16-24 wt. %) with $Mg^{\#}$

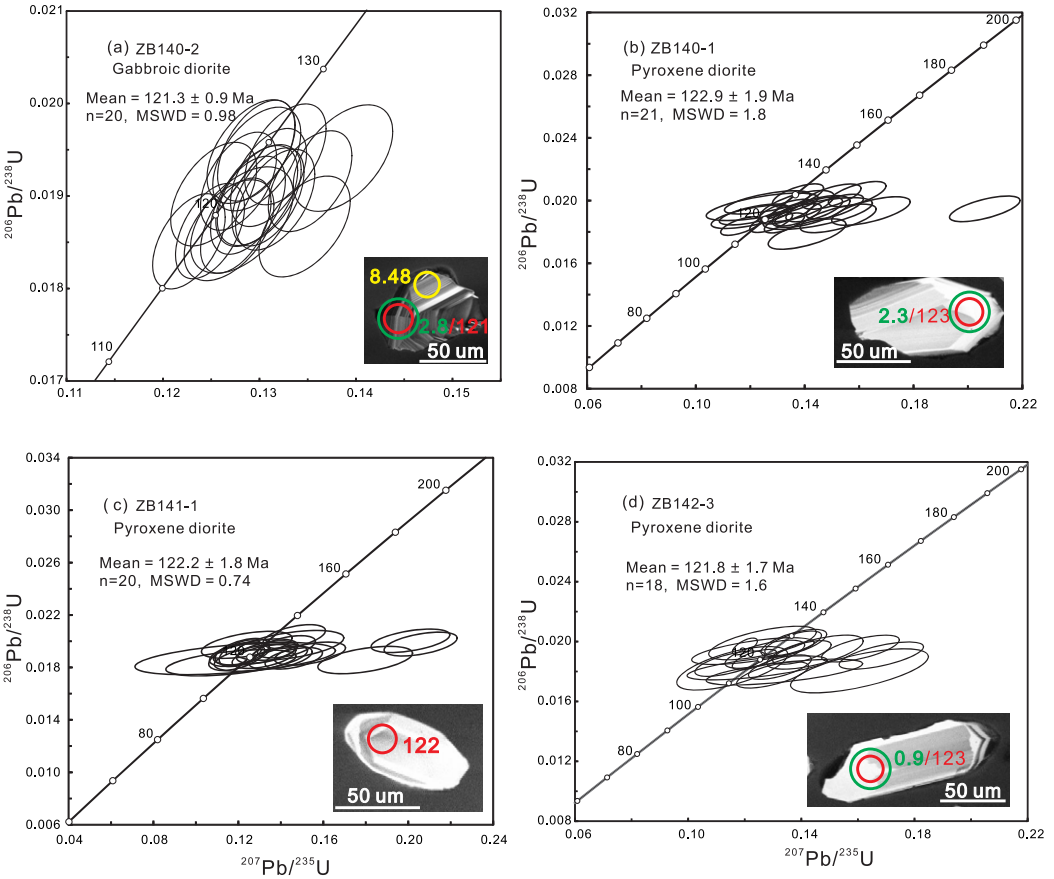

Figure 2. LA–ICP–MS zircon U–Pb Concordia diagrams with representative zircon CL images for the Bizha pluton (a): Gabbroic diorite. (b–d): Pyroxene diorites. The red, yellow, and green circles and numbers denote the analytical spots of U-Pb dating, the analytical spots with zircon $\delta^{18}O$ values, and the analytical spots of Lu-Hf isotopes, respectively.

$(Mg^{2+}/(Fe^{2+}+Mg^{2+}) \times 100)$ values of 52-68. All amphiboles in the Bizha intrusive rocks are calcic and plot in the magnesiohornblende field. Plagioclase grains in the Bizha pluton have variable compositions with An contents ranging from 30 to 90 mol. % but are dominated by andesines and labradorites. Alkali feldspar grains are sanidine and anorthoclase. Micas in the Bizha pluton can be classified as eastonite and annite.

3.3. Major and Trace Element Compositions

Approximately contemporaneous andesitic lavas in the Duolong-Gerze area, including andesites (~124 Ma) from the northern Gerze [*S. Liu et al.*, 2012] and basaltic andesites (~118 Ma) from the Duolong porphyry Cu–Au deposit [*Li et al.*, 2008, 2013], are shown for comparison (Figures 3 and 4).

The Bizha intrusive rocks consist of gabbroic diorites and pyroxene diorites that have SiO_2 contents ranging from 53.2 to 61.2 wt. % (volatile-free) (Figure 3). Compared to the contemporaneous andesitic lavas, the Bizha dioritic rocks exhibit lower total alkalis but similar K_2O contents (Figures 3a and 3b). The Bizha dioritic rocks are dominantly metaluminous as indicated by the aluminum saturation index [$A/CNK = Al_2O_3/(CaO + Na_2O + K_2O)$] (0.77–0.97) with the exception of one sample (1.07). They have moderate MgO contents (2.5–4.7 wt. %) and $Mg^{\#}$ (42–48). The Bizha dioritic rocks and the Duolong-Gerze andesitic lavas define coherent variation trends. MgO, TiO_2, Fe_2O_3T, and CaO show decreasing trends with increasing SiO_2, whereas Al_2O_3 and K_2O show flat trends (Figures 3b–3h). All of the dioritic/andesitic rocks belong to the medium-K and high-K calc-alkaline series (Figure 3b).

On chondrite-normalized REE diagrams, the Bizha dioritic rocks show enrichment of LREE (light rare earth element) with $(La/Yb)_N = 8.7–12.1$ (Figure 4a) and weakly negative Eu anomalies ($Eu/Eu^* (EuN/\sqrt[2]{SmN \times GdN}) = 0.76–0.91$) (Figure 4a). The primitive mantle-normalized trace-element distribution

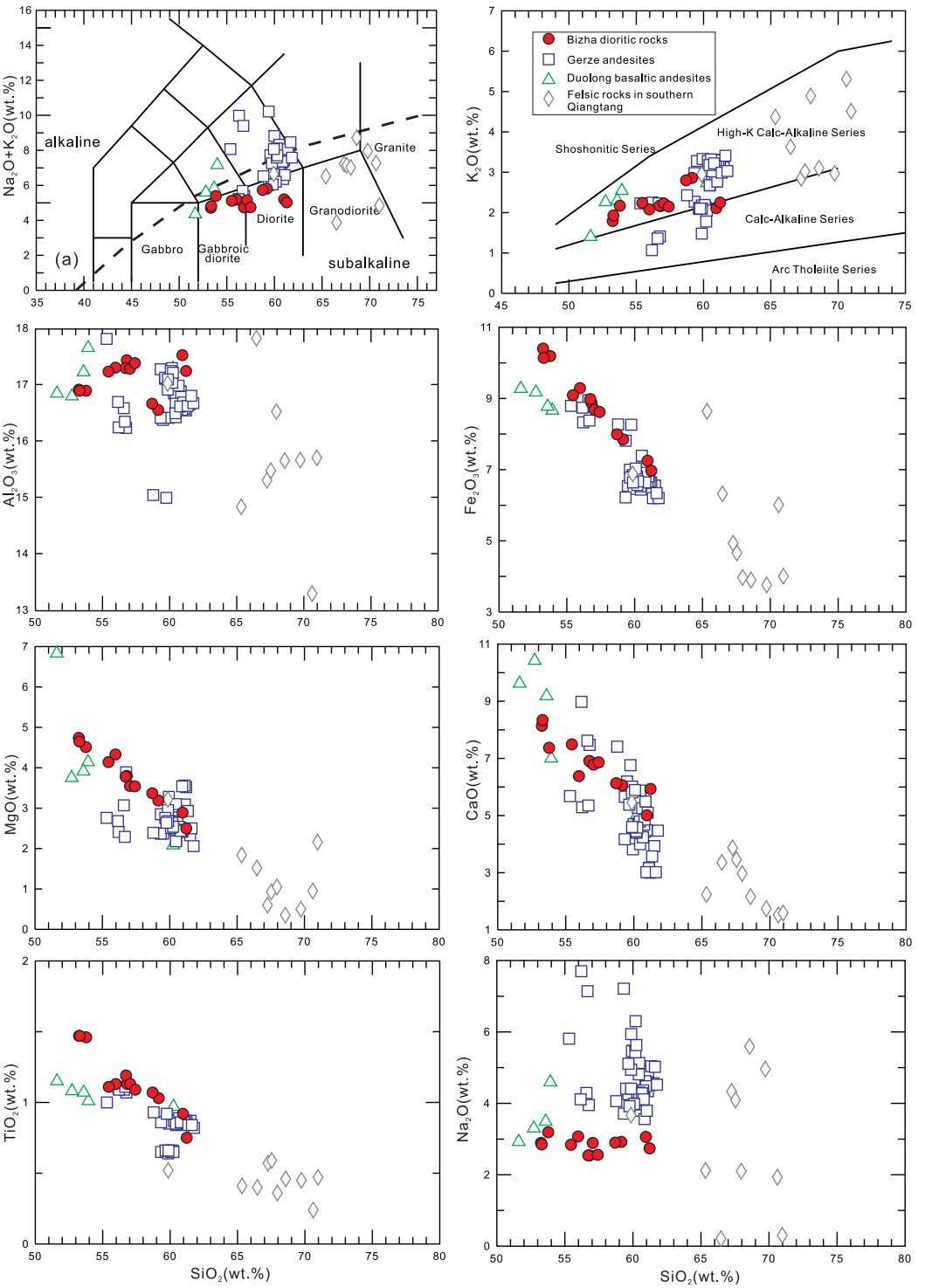

Figure 3. Major element diagrams. (a) TAS classification diagram [*Middlemost*, 1994]. (b–h) Harker diagrams. The Gerze andesites [*D. Liu et al.*, 2012] and the Duolong basaltic andesites [*Li et al.*, 2008, 2013] are shown for comparison. The felsic rocks in southern Qiangtang are from *Li et al.* [2013] and *Hao et al.* [2016].

patterns of the Bizha dioritic rocks are characterized by the enrichment of large ion lithophile elements (LILEs) (e.g., Cs, Rb, Th, Pb, and Ba) and the depletion of high field strength elements (HFSEs) (e.g., Nb, Ta, and Ti) (Figure 4b). The dioritic rocks and andesitic lavas are very similar in their REE (rare earth element) and trace element patterns (Figure 4).

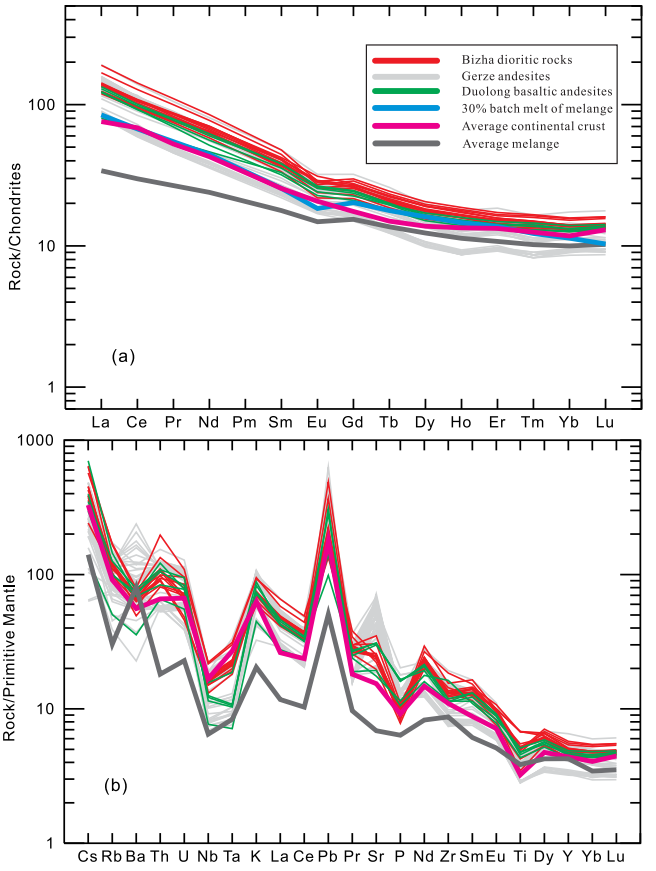

Figure 4. Chondrite-normalized REE patterns (a) and primitive mantle normalized trace element diagrams (b) for the Bizha dioritic rocks. Chondrite and primitive mantle normalized values are from *Sun and McDonough* [1989]. The average mélange composition is from *Bulle et al*. [2010] and the average bulk continental crust composition is from *Rudnick* [1995]. REE patterns of 30% batch partial melts of the mélange are shown. Bulk solid/melt partition coefficients of andesitic melts in equilibrium with the mineral assemblages (15% Cpx, 10% Pl, and 65% Amph, and 10% Grt). Individual mineral Kd values are from *McKenzie and O'Nions* [1991].

3.4. Sr–Nd–Hf-O Isotope Compositions

The whole-rock initial Sr–Nd isotopic ratios were calculated for the emplacement age of 122 Ma. The Bizha dioritic rocks show εNd(t) values ranging from -0.01 to -3.31 and initial $^{87}Sr/^{86}Sr$ isotopic ratios ranging from 0.7053 to 0.7062 (Figure 5a). These Sr-Nd isotope compositions are similar to those of the Early Cretaceous magmatic rocks [*Hao et al*., 2016; *Li et al*., 2008, 2013; *D. Liu et al*., 2014; *S. Liu et al*., 2012], but contrast with those of the Late Jurassic magmatic rocks, which have high initial $^{87}Sr/^{86}Sr$ ($>$ 0.7065) and low εNd(t) values (-3 to -8) [*Hao et al*., 2016; *D. Liu et al*., 2014; *Zhang et al*., 2012, and references therein.) (Figure 5a).

Zircon Hf isotopic analyses were made for three of the four samples that were previously analyzed for U–Pb dating. Zircon Hf isotopic data are illustrated in Figures 5c–5f. Nineteen analyses were made on magmatic zircons from gabbroic diorite sample ZB140-2, yielding εHf(t) values of -2.3 to $+3.6$ (Figure 5c). Twenty analyses on zircons from the pyroxene diorite sample ZB140-1 give ε_{Hf}(t) values of -2.5 to $+2.6$ (Figure 5f). Nine analyses on zircons from the pyroxene diorite sample ZB142-3 give ε_{Hf}(t) values of -5.3 to 2.7 (Figure 5d).

Some O isotope analyses were carried out on magmatic zircon grains for which age and Hf isotope compositions had previously been determined. Additional O isotope analyses were also carried out on undated magmatic zircon grains. The crystal morphology of undated zircons closely resembles those of grains previously analyzed for U-Pb and Hf, and the O isotope analyses yield similar results to those of the dated zircons. Given that no xenocrystic zircons were found in this study, it is reasonable to consider the O isotope data from undated zircons to also represent characteristics of the Bizha pluton. The $\delta^{18}O$ values for zircons from samples ZB140-2, ZB140-1, and ZB141-1 show ranges of $+7.9\sim +8.5‰$, $+7.6\sim +9.5‰$, $+7.3\sim +9.4‰$, forming normal Gaussian distributions, with averaged values of $+8.24 \pm 0.10‰$ (1SD), $+8.46 \pm 0.25‰$ (1SD), and $+8.50 \pm 0.28‰$ (1SD), respectively (Figure 5b). Taken together, the zircon $\delta^{18}O$ values of the Bizha pluton range from $+7.3$ to $+9.5‰$ with a weighted mean values of $+8.4‰$ (Figure 5b), clearly higher than those of $+5.3 \pm 0.3‰$ for normal mantle zircons [*Valley et al*., 1998].

4. Discussion

4.1. Tectonic Setting

Most recent studies have argued that the Bangong-Nujiang Ocean survived until the Late Cretaceous. For example, studies on ophiolitic mélanges of the Bangong-Nujiang Suture (BNS) (Figures 1a and 1b) indicate numerous Early Cretaceous oceanic basalts [e.g., *Bao et al*., 2007; *Baxter et al*., 2009; *Fan et al*., 2014; *K. J. Zhang et al*., 2014; *Zhu et al*., 2006]. In addition, an angular unconformity separates the Late Cretaceous

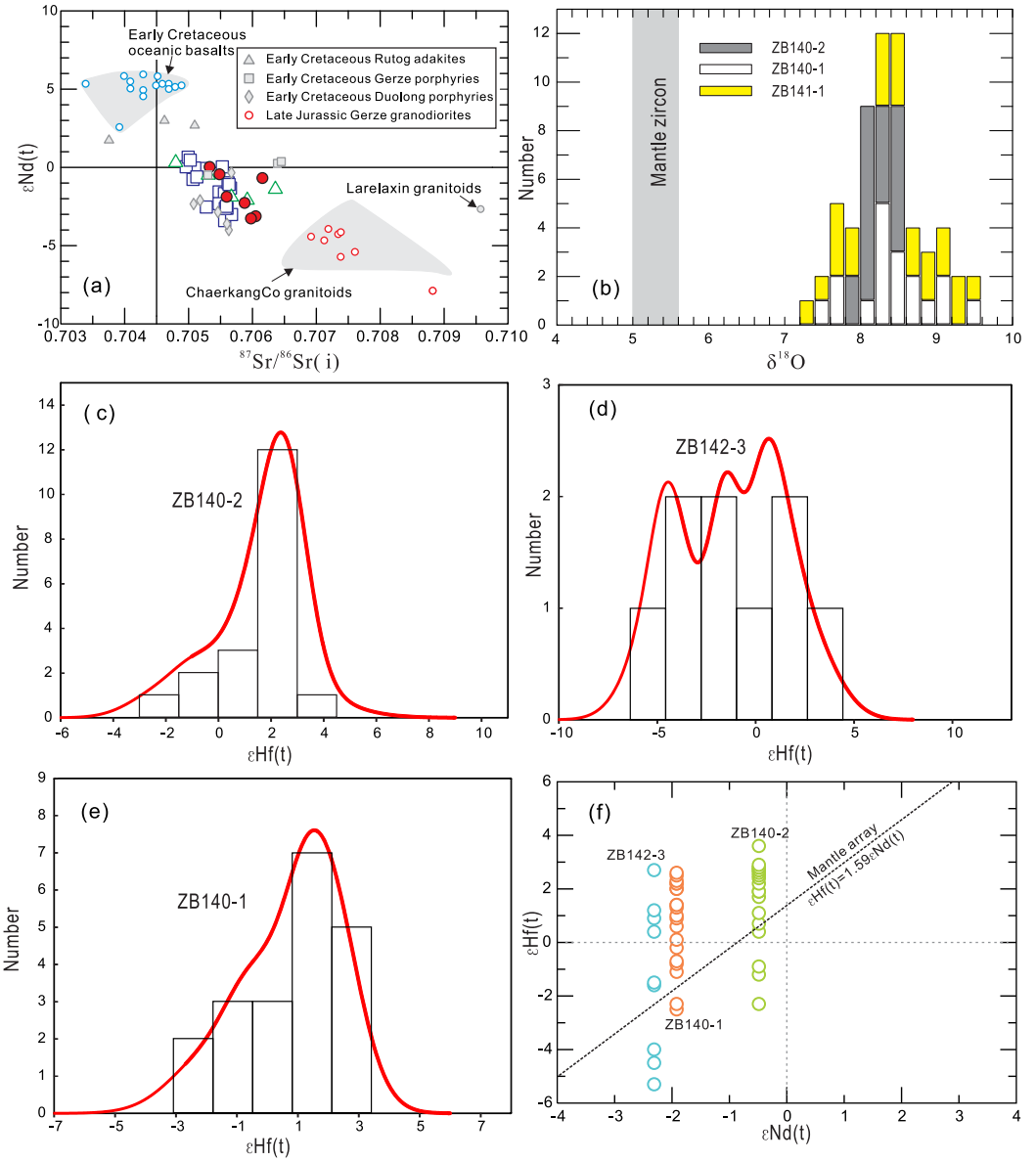

Figure 5. Sr-Nd-Hf-O isotopes. (a) εNd(t) versus ($^{87}Sr/^{86}Sr$)i. Data for the oceanic basalts are from *Bao et al.* [2007] and *Wang et al.* [2016]. Data for the Rutog adakites and Larelaxin intrusive rocks, Duolong granodiorite porphyries, Gerze granodiorites and granodiorite porphyries, and ChaerkangCo granitoids are from *D. Liu et al.* [2014], *Li et al.* [2013], *Hao et al.* [2016] *Zhang et al.* [2012], and references therein, respectively. Note that Sr and Nd isotopic data are all corrected to 122 Ma. (b) Histogram of zircon $\delta^{18}O$ values. (c–e) Histograms of $\varepsilon_{Hf}(t)$ values. (f) Zircon εHf(t) versus whole-rock εNd(t) diagram. Mantle array are from *Chauvel et al.* [2008].

Jingzhushan formation, which displays the characteristics of continental deposits, from the underlying ophiolites [e.g., *Xu et al.*, 2014]. A recent sedimentological study also indicates that the Bangong-Nujiang ocean closed at ~100 Ma [*Fan et al.*, 2015] rather than in the Late Jurassic-Early Cretaceous (~145 Ma) [e.g., *Zhu et al.*, 2011], consistent with a continental arc setting. Therefore, the extensive (>1000 km long) Late Mesozoic continental arc magmatism (170–102 Ma) in southern Qiangtang to the north of BNS should be attributed to the northward subduction of the Bangong-Nujiang Ocean.

4.2. Petrogenesis

The Early Cretaceous (124–118 Ma) intermediate (andesitic/dioritic) rocks in southern Qiangtang, including the Bizha dioritic rocks (this study), the northern Gerze andesites [*S. Liu et al.*, 2012], and the Duolong basaltic andesites [*Li et al.*, 2008, 2013] can be considered collectively due to their regular variations on Harker diagrams (Figure 3), the similarity of their REE and trace element patterns (Figure 4) and their consistent

Sr-Nd isotopic compositions (Figure 5a). These approximately contemporaneous intermediate rocks most plausibly have a common source and petrogenesis.

4.2.1. Crustal Assimilation and Fractional Crystallization

Significant crustal contamination for these intermediate rocks can be ruled out given that: (1) Crustal assimilation and fractional crystallization (e.g., AFC process) generally lead to strong correlations between indices of fractionation (e.g., SiO_2, MgO, $Mg^{\#}$ values, Sm/Nd) and the chemical/or isotope data (Sr-Nd-Hf-O isotopes) because of the significant differences between the mantle and crust [e.g., *Xu et al*., 2004]. However, the intermediate rocks as a whole do not generally show such regular correlations (Figures 6a–6e). Moreover, both the Bizha dioritic rocks and the Gerze andesites show limited ranges of whole-rock Sr isotopic compositions (Figures 6a and 6c). (2) Most samples have incompatible element contents significantly higher than the upper continental crust. (3) There are no zircon xenocrysts in the Bizha dioritic rocks; (4) Simple mixing modeling results show that in order to change the highest $\varepsilon Nd(t)$ value ($= 0$) of the basaltic andesites to the lowest $\varepsilon Nd(t)$ value ($= -3.5$), an assimilation of up to 40% of lower crust material is required (Figure 6f). Involvement of such a high percentage of crustal material would form felsic rocks, like the Duolong felsic porphyries, rather than these intermediate rocks [e.g., *Li et al*., 2013], and can, therefore, be excluded. The Duolong felsic porphyries generated by mixing between lower crust and basaltic melts [e.g., *Li et al*., 2013] have similar Sr-Nd isotopic compositions but higher SiO_2 contents (58.8–68.8 wt. %) when compared with the studied intermediate rocks. In addition, the Amdo gneisses near southern Qiangtang are characterized by strongly enriched $(^{87}Sr/^{86}Sr)_i$ values ($\sim$0.74) [*Harrison et al*., 1992] (Figure 6f) and could not have been one of the contaminants, otherwise contamination would have resulted in high $(^{87}Sr/^{86}Sr)_i$ values for intermediate rocks. (5) The cores and rims of the mafic minerals (e.g., pyroxene and amphibole) do not show obvious compositional variations, also inconsistent with crustal contamination. Therefore, the intermediate rocks are unlikely to have suffered significant crustal contamination during their ascent and emplacement.

The major-element covariations in these intermediate rocks could not have been caused by fractional crystallization (FC), because a FC process cannot explain the heterogeneity of the Sr-Nd-Hf isotopes (Figure 5). In addition, a FC process requires a corresponding abundance of basalts and gabbros, given the quantitative consideration of volume proportions between the parental and evolved magmas [*Zheng et al*., 2015]. However, contemporaneous basaltic rocks are scarce in southern Qiangtang. Furthermore, on a diagram of La versus La/Yb (Figure 5g), the intermediate rocks, particularly the more mafic members, fall along the path of partial melting rather than fractional crystallization.

Based on these considerations, we conclude that the compositions of the andesitic/dioritic rocks in southern Qiangtang were mainly generated by partial melting of their source rocks. Therefore, their heterogeneous geochemical features are inherited from their magma sources and can be used to constrain the nature of those sources.

4.2.2. Involvement of Sediments in the Magma Source

The more mafic examples of these intermediate rocks have low silica ($SiO_2 < 57$ wt. %) and relatively high MgO ($>$3 wt. %) contents and $Mg^{\#}$ (> 45). Experimental data show that partial melts of basalts typically show low $Mg^{\#}$ (< 41) regardless of the degree of melting [e.g., *Rapp and Watson*, 1995]. It is evident from Figure 6h that the Mg numbers ($Mg^{\#}$) of the intermediate rocks are distinctly higher than experimental crustal melts and that the intermediate rocks have significantly lower SiO_2 contents and higher $Mg^{\#}$ than lower continental crust-derived rocks such as the Gerze granodiorites and granodiorite porphyries [*Hao et al*., 2016], or the Larelaxin intrusive rocks [*D. Liu et al*., 2014]. Therefore, we suggest that the sources of intermediate rocks were mafic-ultramafic mantle lithologies rather than mafic-felsic crustal lithologies.

However, there are lines of important evidence for involvement of sediments in the magma source. First, the intermediate rocks exhibit lower contents of MgO and compatible trace elements (e.g., Cr and Ni) than normal mid-ocean ridge basalts (MORBs) that are attributed to partial melting of the normal asthenospheric mantle. Second, they exhibit arc-like trace element distribution patterns such as enrichment of LILEs, Pb, and LREE but the depletion of HFSEs (Figure 4). Besides, the Nb/La and Ce/Pb ratios of these intermediate rocks are intermediate between those of the subducted sediments and the oceanic basalts (Figure 7a). Furthermore, compared to contemporaneous oceanic basalts in the Bangong-Nujiang ophiolite suites [*Bao et al*., 2007; *Wang et al*., 2016], the Bizha dioritic rocks exhibit slightly enriched and variable Sr-Nd isotope compositions, with $\varepsilon Nd(t)$ values of -0.01 to -3.31 and initial $^{87}Sr/^{86}Sr$ isotopic ratios of 0.7053–0.7062 (Figure 5a). More specifically, the Sr-Nd isotopic compositions of the southern Qiangtang intermediate rocks fall

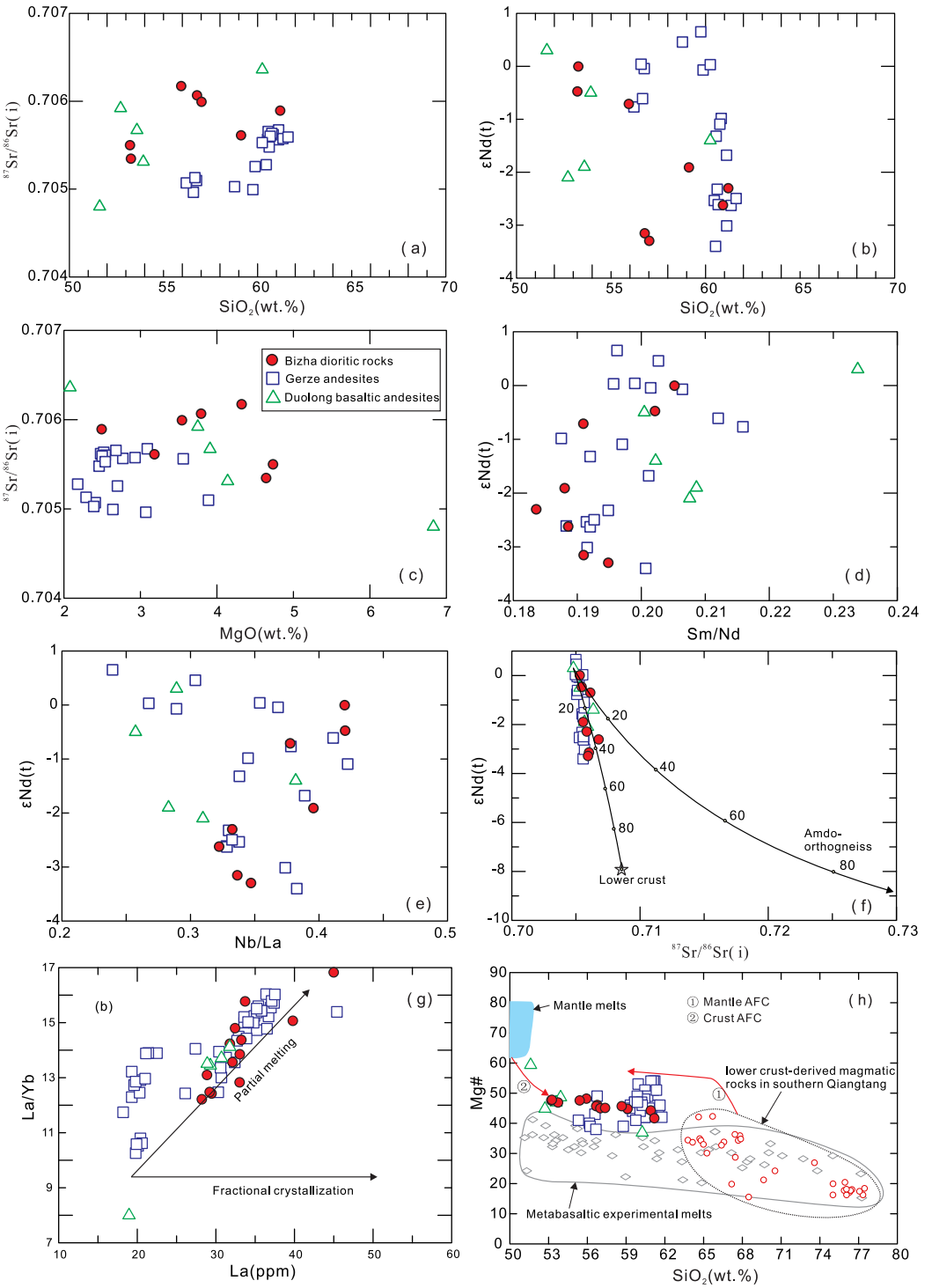

Figure 6. (a–e) Plots of Sr-Nd isotope, element, and elemental ratios of the intermediate rocks. (f) Simple mixing modeling results of the most depleted basaltic andesite [*Li et al.*, 2008] and the lower crust. The lower crust compositions are represented by the northern Gerze granodiorites with the most enriched Sr-Nd [*Hao et al.*, 2016] and the Amdo orthogneiss [*Harrison et al.*, 1992]. (g) La/Yb versus La (ppm). (h) SiO_2 versus $Mg^{\#}$ diagram. Mantle melts, mantle AFC, and crust AFC are from *Wang et al.* [2006] and references therein. Metabasaltic experimental melts are from *Rapp and Watson* [1995]. The lower crust-derived magmatic rocks are from *Hao et al.* [2016] and *D. Liu et al.* [2014].

between those of the subducted sediments and oceanic basalts (Figure 7b). In addition, they also have variable magmatic zircon Hf-O isotope compositions (εHf(t) = −5.3 to +3.6 and $\delta^{18}O$ = +7.3 to +9.5 ‰) (Figures 5b–5f). On a plot of εNd(t) versus zircon εHf(t) (Figure 5f), the Bizha dioritic rocks plot close to the

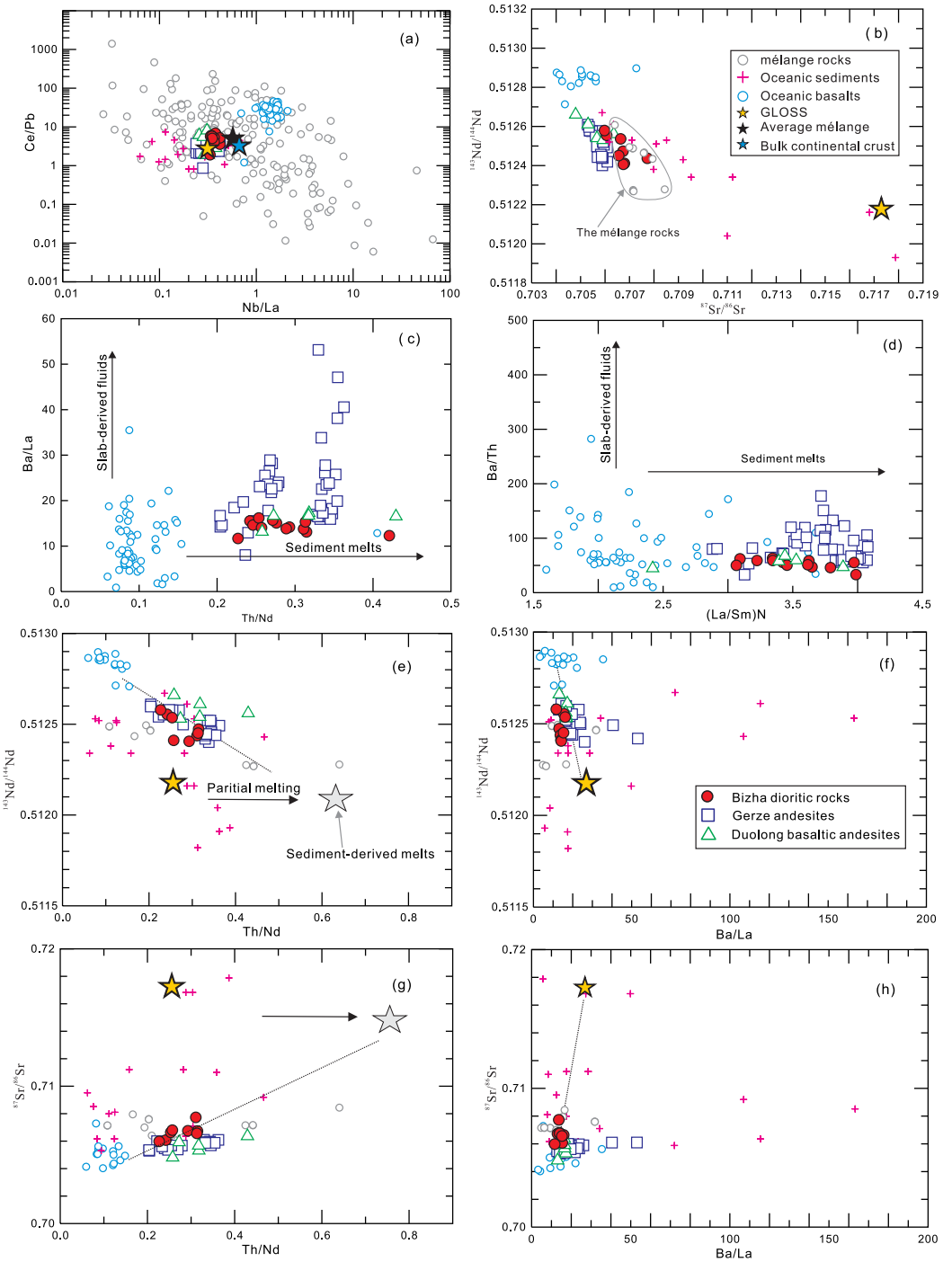

Figure 7. (a) Ce/Pb versus Nb/La plot for the intermediate rocks. Mélange rocks are from *Bulle et al.* [2010]. The oceanic sediments and GLOSS are from *Plank and Langmuir* [1998]. The bulk continental crust (BCC) is from *Rudnick* [1995]. The oceanic basalts are from *Bao et al.* [2007] and *Wang et al.* [2016]. (b) $^{87}Sr/^{86}Sr$ versus $^{143}Nd/^{144}Nd$ for the intermediate rocks, oceanic sediments, and basalts, the melange rocks. (c) Ba/La versus Th/Nd. (d) Ba/Th versus $(La/Sm)_N$. (e and f) $^{143}Nd/^{144}Nd$ versus Th/Nd and Ba/La. (g-h) $^{87}Sr/^{86}Sr$ versus Th/Nd and Ba/La. The dotted lines in Figures 7e–7h show the linear arrays.

mantle array. *Chauvel et al.* [2008] demonstrated the role of recycled sediment components in generating the Hf-Nd mantle array but did not specify the form of the sediment component. Because significant crustal contamination of the magma in the overriding plate can be ruled out as mentioned above, all of these "continental crust-like" geochemical features indicate that the magma sources of the intermediate rocks contain

significant amounts of subducted sediments, which slab subduction can efficiently carry into the mantle in a continental arc.

The subducted sediment components would be present in the forms of aqueous fluids, hydrous melts, or bulk sediment [*Class et al*., 2000]. We suggest that bulk sediment rather than aqueous fluids or sediment melts was most probably incorporated into the magma source of these intermediate rocks based on following observations. First, the rocks have significantly higher Th/Nd ratios (Figure 7c) than the asthenosphere-derived oceanic basalts [*Bao et al*., 2007; *Wang et al*., 2016], which argues against a dominantly aqueous fluid sediment component. Such fluids carry very little REE, Th, and HFSE (e.g., Hf, Nb, Zr, and Ta) but significant amounts of large ion lithophile elements (e.g., K, Rb, Ba, and Sr) and other fluid-mobile trace elements (e.g., U, Pb) [e.g., *Guo et al*., 2013], which should lead to decreased Th/Nd ratios. On a plot of $(La/Sm)_N$ versus Ba/Th, commonly invoked to illustrate the contribution of a crustal component to the source region of arc volcanic rocks in three-component mixing [e.g., *Elliott et al*., 1997] (Figure 7d), the intermediate rocks also show higher $(La/Sm)_N$ values than oceanic basalts. The common explanation is that the trend to high $(La/Sm)_N$ at low Ba/Th values results from the addition of sediments to the magma source, whereas the trend to high Ba/Th values at low $(La/Sm)_N$ values is attributed to dehydration of altered oceanic crust [e.g., *Elliott et al*., 1997]. In addition, the combination of incompatible elements and isotopic ratios has also been effectively used as a fingerprint in identifying the origin of mixed end-members in magma sources [e.g., *Class et al*., 2000]. The intermediate rocks form approximately linear arrays on plots of $^{143}Nd/^{144}Nd$ and $^{87}Sr/^{86}Sr$ versus Ba/La, consistent with control by source mixing (Figures 7f and 7h). One of the end members must be bulk sediment or sediment melts (Figures 7f and 7h) rather than aqueous fluids because fluids will strongly fractionate the fluid-mobile element Ba and fluid-immobile element La and lead to an increased Ba/La ratio. Likewise, we can infer from plots of $^{143}Nd/^{144}Nd$ and $^{87}Sr/^{86}Sr$ versus Th/Nd (Figures 7e and 7g) that one of the end-members is likely to be sediment melts or bulk sediment rather than aqueous fluids, given that aqueous fluids cannot fractionate the fluid-immobile elements Th and Nd [*Johnson and Plank*, 1999]. Finally, the high zircon $\delta^{18}O$ values of the Bizha dioritic rocks (Figure 5b) suggest substantial incorporation of bulk sediment into their magma source because aqueous fluids and small proportions of slab-derived melts cannot significantly change the O isotopic compositions of a magma source in subduction zones [e.g., *Eiler*, 2001]. Therefore, we prefer the incorporation of bulk sediment, in solid form, rather than sediment melts involved in magma source (see discussions below).

4.2.3. Partial Melting of Mélange to Produce Intermediate Magmas

The evidence for oceanic basalts, mantle wedge, and subducted sediment in the magma source of the intermediate rocks is broadly consistent with the two classic slab-mantle reaction models in subduction zones [e.g., *Castro et al*., 2010, 2013; *Kelemen*, 1995; *Zheng*, 2012]. In the classic models, the mantle was either metasomatized by felsic melts and then served as a source for arc magmas or by slab-derived melts that react with the mantle to directly produce arc magmas [e.g., *Castro et al*., 2010, 2013; *Kelemen*, 1995; *Zheng*, 2012]. Resolving the specific mechanism for the transfer of slab and sediment components into the mantle wedge is a key requirement to understanding the petrogenesis of the southern Qiangtang intermediate rocks.

Recently, a combination of results from the studies of high-pressure metamorphic rocks in mélange zones, numerical modeling, geophysics, and geochemistry suggests a two-step process by which components from a subducting slab and overlying mantle wedge can be transported into the magma source of subduction-related magmas [*Marschall and Schumacher*, 2012]. First, the intensely mixed metamorphic rock formations, i.e., mélanges, form along the interface between the subducted slab and the mantle in the subduction channel where mantle rocks are mixed with material derived from the subducting slab, including trench sediments. Then, diapirs of low-density mélange material rise buoyantly from the surface of the subducting slab and transport the well-mixed mélange material into the mantle beneath a volcanic front. As the mélange contains both depleted (oceanic basalts and mantle wedge peridotites) and enriched (subducted sediments) components, mélange diapir-related melts exhibit the characteristic subduction-zone magmas geochemical patterns, such as the distinctive enrichment in LILEs and the significant depletion in HFSEs [*Marschall and Schumacher*, 2012]. An important difference between the mélange-diapir model and the classic slab-mantle reaction model lies in the relative order of events: mixing followed by mixture melting versus slab melting followed by mixing, respectively. The mélange-diapir model best explains the specific slab-mantle mixing process responsible for arc magmas.

In this study, we have adapted the mélange-diapir model [*Marschall and Schumacher*, 2012] for the petrogenesis of the intermediate rocks in southern Qiangtang, Tibet, and our results validate its main premise.

Like the Bizha dioritic rocks, Gerze andesites, and Duolong basaltic andesites, mélange rocks display enrichments in LILE, LREE, and depletions in HFSE, including significant positive Pb anomalies and negative Nb, Ta, and Ti anomalies, and show similar REE patterns and spidergrams (Figure 4). These shared characteristics indicate mélange rocks are a potential source for the intermediate magmatic rocks, consistent with their comparable Nb/La and Ce/Pb (Figure 7a). In addition, mélange rocks are more mafic or less ultramafic than mantle peridotite in their major-element compositions and can partially melt to form the intermediate rocks [e.g., *Castro et al*., 2010]. Moreover, the intermediate rocks have Sr-Nd isotopic compositions comparable to mélange rocks in Andros investigated by *Bulle et al*. [2010] (Figure 7b), which are slightly enriched relative to the depleted mantle and oceanic basalts. In addition, simple REE data modeling shows that 30% batch partial melting of average mélange can produce REE patterns similar to those of the intermediate rocks (Figure 4a).

Accordingly, we suggest that the Bizha dioritic rocks, Gerze andesites and Duolong basaltic andesites were derived from a subduction mélange.

5. Geodynamic Processes and Implications for Crustal Growth

5.1. Geodynamic Processes

As argued above, the Late Mesozoic magmatism in southern Qiangtang was due to northward subduction of the Bangong-Nujiang Ocean [*Hao et al*., 2016; *Zhu et al*., 2016]. However, the specific geodynamic process responsible for the Early Cretaceous magmatism has not been clear.

It should be noted that from the Late Jurassic to Early Cretaceous, there is a noticeable ~20 Ma magmatic gap (145–125 Ma) (Figure 8a). Similar magmatic lulls occur in the Andes and southern Gangdese areas in response to low-angle subduction [e.g., *Ma et al*., 2013]. The renewed magmatism following this gap is considered to be the product of slab roll-back (a rapid steepening of the subducting slab). Here, we have adapted this model for the southern Qiangtang geodynamic setting and suggest that the Early Cretaceous magmatism was a result of slab roll-back.

There is additional evidence for slab roll-back. First, during the transition from flat to normal angle subduction, upwelling asthenospheric mantle, and hot corner flow would have provided the heat source for partial melting of mélange rocks, and the lower crust. This would readily account for the magmatic flare-up in the Early Cretaceous in southern Qiangtang (Figure 8a). High crystallization temperatures (982–1077°C) of the Bizha dioritic rocks obtained using the two-pyroxene geothermometer [*Taylor*, 1998] indicate a high temperature, consistent with such asthenospheric upwelling. Second, slab roll-back would have been accompanied by a southward migration of asthenospheric convection beneath southern Qiangtang, which induced a corresponding southward migration of magmatism during the Early Cretaceous. As shown in Figure 8a, the Late Jurassic magmatic rocks occurred in the north of southern Qiangtang, far from the subduction zone, suggesting that the subducted plate frontier moved further north probably due to low-angle subduction. Early Cretaceous magmatic rocks were widely distributed across the whole southern Qiangtang, regardless of the distance to the subduction zone, and this time-space distribution is consistent with slab roll-back (Figure 8a). Third, slab roll-back would also have led to the rifting and extension within the overriding plate [e.g., *Tang et al*., 2012]. In this regard, a recent study has reported ~122 Ma bimodal volcanic rocks in the Maierze area, southern Qiangtang, which are considered to have formed during the initial development of an extensional setting [*Fan et al*., 2015].

Based on these factors, we suggest that the Early Cretaceous southern Qiangtang magmatism was the product of slab roll-back during northward subduction of the Bangong-Nujiang Ocean and that the intermediate rocks were generated by partial melting of mélange rocks in this scenario (Figure 9).

Although mélange rocks may melt during steady state subduction [*Guo et al*., 2014], the complex succession of flat-slab subduction and slab roll-back in our tectonic model may promote the process. During flat-slab subduction, as in an Andes-type subduction zone, large amounts of sediment could easily be subducted into mantle by subduction erosion [e.g., *von Huene and Scholl*, 1991]. In this flat-slab setting, however, the cold wedge and lack of corner flow inhibits sediment melting. Subsequent asthenospheric upwelling and hot corner flow during slab roll-back (~124 Ma) would drastically change the thermal state of the wedge

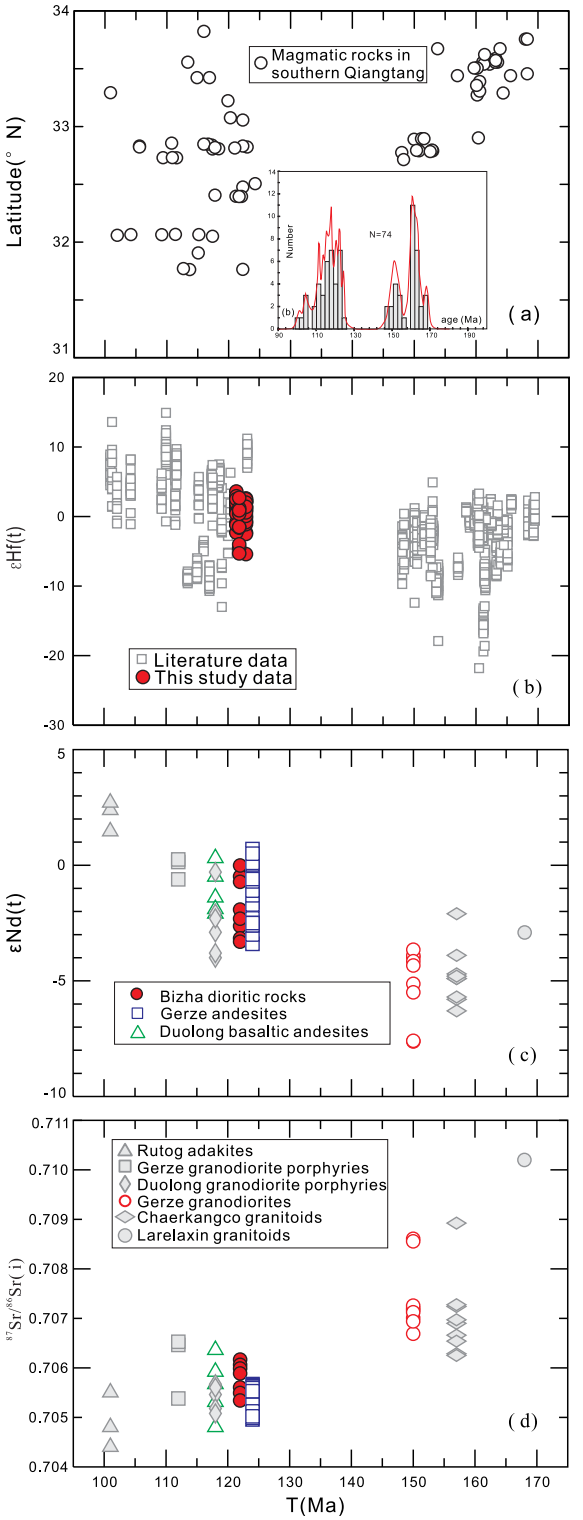

Figure 8. Time-space distribution and Sr-Nd-Hf isotope variations for the Late Mesozoic southern Qiangtang magmatic rocks. (a) U-Pb ages of magmatic rocks plotted against their latitudes. The inset shows the histogram of age data. (b–d) Plots of εHf(t), εNd(t), and ($^{87}Sr/^{86}Sr$)i versus T (Ma). The age and location data, Sr-Nd-Hf isotope data are from: *Chang et al.* [2011]; *Fan et al.* [2015]; *Hao et al.* [2016]; *Kapp et al.* [2005]; *J. X. Li et al.* [2013, 2014]; *S.-M. Li et al.* [2014]; *D. Liu et al.* [2014, 2015]; *S. Liu et al.* [2012]; *Zhang et al.* [2012]; and references therein; and this study.

leading to the partial melting of large volumes of mélange rocks to produce a magmatic flare-up and increased production of intermediate rocks as observed in southern Qiangtang (Figure 9b).

5.2. Partial Melting of Mélange for Crustal Growth

It is widely accepted modern continental crust is dominantly created at convergent margins [e.g., *Rudnick*, 1995]. Phanerozoic continental crustal growth primarily occurs in subduction zones by lateral accretion of island or intraoceanic arc complexes and oceanic plateaus or by vertical addition by underplated magmas that could be either basaltic or andesitic melts [e.g., *Rudnick*, 1995; *Castro et al.*, 2013]. It has long been recognized, however, that individual active subduction zones may not be sites for net continental growth because *von Huene and Scholl* [1991] demonstrated quantitatively that crustal addition by subduction zone magmatism may be mass balanced by crustal loss through sediment subduction and subduction erosion. Accordingly, Phanerozoic continental crustal growth generally refers to significant formation of continental crust.

Recently, *Hao et al.* [2016] suggested vertical crustal growth by magma underplating for a southern Qiangtang continental arc, based on the tracking of the magma sources of the Late Mesozoic intermediate-felsic intrusive rocks in southern Qiangtang. As illustrated in Figures 8b–8d, the Late Jurassic magmatic rocks in southern Qiangtang generally exhibit enriched Sr-Nd and zircon Hf isotopic compositions while the Early Cretaceous magmatic rocks primarily have relatively depleted Sr-Nd and zircon Hf isotopic compositions. Therefore, *Hao et al.* [2016] inferred that ancient lower crust was gradually replaced by younger materials between the Late Jurassic to Early Cretaceous, consistent with vertical crustal growth by magma underplating. However, the nature of the underplated magmas was unknown.

As discussed above, scarce basaltic rocks and abundant intermediate-felsic rocks occurred in southern Qiangtang which was located in a continental arc in Late Mesozoic. Here, we suggest that the young crust may be underplated andesitic magmas, and that the Bizha

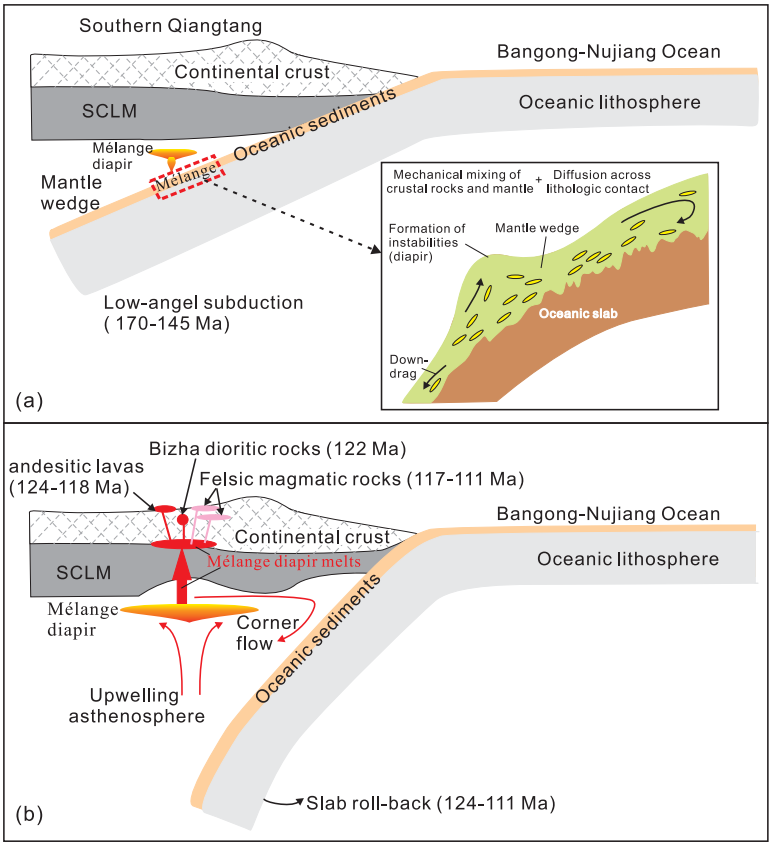

Figure 9. A conceptual model illustrating the tectonic evolution and magmatism in southern Qiangtang during the Late Mesozoic. (a) A low-angel subduction of the Bangong-Nujiang Ocean during the Late Jurassic (170–145 Ma). The inset shows that the mélange formation (modified from the diagram of *Marschall and Schumacher* [2012]). The mélange rises buoyantly in a form of diapir from the surface of the slab into the mantle wedge due to the instabilities. (b) During the transition from flat to normal angle subduction at 124 Ma, upwelling asthenospheric mantle and hot corner flow provided the heat source for the partial melting of mélange diapir. Partial melting of the mélange diapir then formed the underplated andesites. Some melts erupted to form the andesitic lavas (124-118 Ma) and some melts were emplaced within the crust to form the dioritic rocks (e.g., the ~122 Ma Bizha intrusive rocks in this study). Such underplated andesites represent the young continental crust and can further form later felsic magmatic rocks (117-112 Ma) by partially melting or by AFC process in the Duolong-Gerze area (e.g., the Duolong and Gerze granodiorite porphyries).

dioritic rocks, Gerze andesites, and Duolong basaltic andesites are the product of this underplating. Their generally andesitic chemical compositions with average SiO_2 of 58.9 wt. %, K_2O of 2.1 wt. %, and $Mg^{\#}$ of 49 overlap those of high-$Mg^{\#}$ andesitic lavas and plutonic rocks in subduction-related magmatic arcs, with SiO_2 of 57–65 wt. %, K_2O of 0.96–2.89 wt. % and $Mg^{\#}$ of 45–54 [*Kelemen*, 1995]. Their REE patterns and spidergrams are also identical to average continental crust (Figure 4). Therefore, the intermediate rocks derived by partial melting of mélange rocks, with continental crust-like andesitic compositions, provide important support for the generation of andesite magmas in arcs and the andesite model of crustal growth. The significant sedimentary component in the mélange rocks also accounts for the enriched Sr-Nd and zircon Hf isotopic compositions of these rocks (Figures 8b–8d). The mélange model emphasizes the important role of recycled sediments in the generation of Phanerozoic andesitic continental crustal, consistent with the andesite model [e.g., *Castro et al*., 2010, 2013; *Zheng*, 2012]. Mass balance calculations for crustal growth at convergent margins incorporate mass loss via the return of sedimentary debris into the mantle [*von Huene and Scholl*, 1991]. The mélange melt model suggests, however, that an additional process can rapidly return significant portions of these sediments to the evolving crust.

5.3. A Test for Our Model

Castro et al. [2013] endorsed the andesite crustal growth model and suggested that andesitic magmas are added to the continental crust, where they partially crystallize separate into a solid fraction to form mafic granulites (lower crust) and granitic liquids to form upper crust batholiths. If the model applies to southern

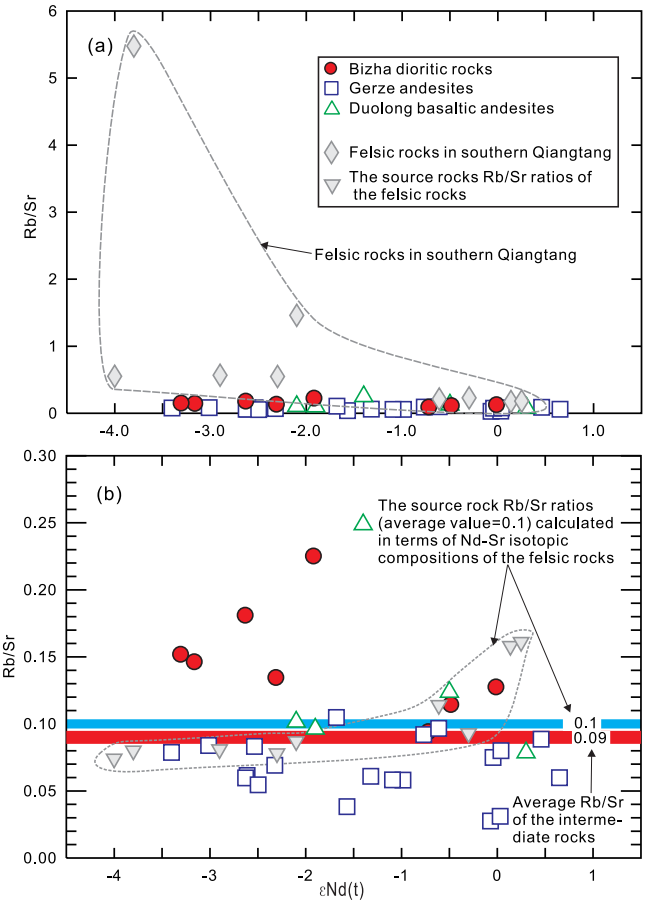

Figure 10. (a) Rb/Sr ratios versus εNd(t) showing the felsic rocks have significantly higher Rb/Sr than the intermediate rocks. (b) Rb/Sr versus εNd(t) showing the source rock Rb/Sr ratios of the felsic rocks are consistent with those of the intermediate rocks. The source rock Rb/Sr ratios were calculated based on the evolution of Sr isotopes in the period between the T_{DM} Nd model age and the crystallization of the samples analyzed [*Dhuime et al.*, 2015]. The felsic rocks in the Gerze-Duolong area include the Gerze granodiorite porphyries (112 Ma) [*Hao et al.*, 2016] and the Duolong granodiorite porphyries (117 Ma) [*Li et al.*, 2013].

Qiangtang, then the Early Cretaceous andesitic/dioritic rocks (124–118 Ma) should also correspond to the parental magmas of the slightly younger (117–112 Ma) felsic rocks in the Duolong-Gerze area.

We can test this model by illuminating the relationship between the Duolong-Gerze intermediate and felsic rocks. Several important facts strongly support a genetic relationship between the two sets of rocks. First, on Harker diagrams, the Duolong-Gerze intermediate rocks, and the more felsic types (the Duolong ore-bearing granodiorite porphyries and the Gerze granodiorite porphyries) define coherent variation trends between K_2O, MgO, TiO_2, Fe_2O_3, CaO, Al_2O_3, P_2O_5, and SiO_2 (Figure 3). This suggests a genetic connection between the intermediate rocks and the more felsic rocks in southern Qiangtang. Besides, the more felsic rocks [*Hao et al.*, 2016; *Li et al.*, 2013] have Sr-Nd-Hf isotopic compositions similar to the intermediate rocks (124–118 Ma) (Figures 5a and 10), suggesting they could plausibly be derived from the intermediate rocks. Moreover, although the felsic rocks have significantly higher Rb/Sr ratios than the intermediate rocks, their source rock Rb/Sr ratios calculated on the basis of Sr isotopic evolution in the period between their T_{DM} Nd model age and crystallization [*Dhuime et al.*, 2015] are nearly identical to those of the intermediate rocks (Figure 10).

In summary, diverse lines of evidence from intermediate and felsic rocks suggest that the young continental crust was newly created by underplating of the andesitic magmas which were derived from mélange diapir partial melting. On this basis, our study strongly supports "the andesite model" for crustal growth.

6. Conclusions

1. The Bizha pluton consists of gabbroic diorites and pyroxene diorites and was emplaced in the Early Cretaceous (~122 Ma), which is approximately contemporaneous with the Duolong-Gerze andesites (~124 Ma) and basaltic andesites (~118 Ma) in southern Qiangtang. The dioritic rocks and andesitic lavas have similar arc-like geochemical characteristics.
2. The Early Cretaceous intermediate magmatic rocks were most probably derived by partial melting of mélange rocks, which was triggered by the upwelling of asthenosphere and hot corner flow caused by roll-back of northward subducted Bangong-Nujiang oceanic slab during Early Cretaceous.
3. The Early Cretaceous intermediate magmatic rocks have an overall continental crust-like andesitic composition in both major and trace elements.
4. The tectonic model involves a complex succession of flat-slab subduction and slab roll-back during which significant amounts of mélange material are formed and subsequently melted when the mantle

wedge heats up due to the steepening of the slab. The intermediate magmas derived by partial melting of mélange rocks may have been underplated at the base of southern Qiangtang and represent young continental crust. They are likely to differentiate in the lower crust to form the felsic intrusions of typical upper crust composition in southern Qiangtang. The mélange model provides important insights into the generation of andesitic magmas in continental arcs and supports the "andesite model" for Phanerozoic continental crustal growth.

Acknowledgments

We are grateful for the constructive comments and suggestions by Editor Ulrich Faul, Horst Marschall, and an anonymous reviewer, which greatly improved the quality of our manuscript. We appreciate the assistance of Yue-Heng Yang, Xi-Rong Liang, Xiang-Lin Tu, Jin-Long Ma, Guang-Qian Hu, Lie-Wen Xie, and Ying Liu for zircon age and geochemical analyses. Financial support for this research was provided by the National Natural Science Foundation of China (41025006), the Strategic Priority Research Program (B) of the Chinese Academy of Sciences (grant XDB03010600), the National Natural Science Foundation of China (41421062), and the Guangzhou Institute of Geochemistry, Chinese Academy of Sciences (GIGCAS 135 project 135TP201601) and the scientific and technical innovation-intersection and cooperation team program of Chinese Academy of Sciences. This is contribution IS-2224 from GIGCAS.

References

Bao, P., X. Xiao, L. Su, and J. Wang (2007), Petrological, geochemical and chronological constraints for the tectonic setting of the Dongco ophiolite in Tibet, *Sci. China. D.*, *50*, 660–671.

Baxter, A. T., J. C. Aitchison, and S. V. Zyabrev (2009), Radiolarian age constraints on Mesotethyan ocean evolution, and their implications for development of the Bangong-Nujiang suture, Tibet, *J.Geol. Soc. London*, *166*, 689–694.

Belousova, E., W. L. Griffin, S. Y. O'reilly, and N. Fisher (2002), Igneous zircon: Trace element composition as an indicator of source rock type, *Contrib. Mineral. Petrol.*, *143*, 602–622.

Bulle, F., M. Bröcker, C. Gärtner, and A. Keasling (2010), Geochemistry and geochronology of HP mélanges from Tinos and Andros, cycladic blueschist belt, Greece, *Lithos*, *117*, 61–81.

Castro, A., T. Gerya, A. García-Casco, C. Fernández, J. Díaz Alvarado, I. Moreno-Ventas, and I. Loew (2010), Melting relations of MORB-sediment mélanges in underplated mantle wedge plumes. Implications for the origin of cordilleran-type batholiths, *J. Petrol.*, *51*, 1267–1295.

Castro, A., K. Vogt, and T. Gerya (2013), Generation of new continental crust by sublithospheric silicic-magma relamination in arcs: A test of *Taylor*'s andesite model, *Gondwana Res.*, *23*, 1554–1566.

Chang, Q. S., D. C. Zhu, Z. D. Zhao, G. C. Dong, X. X. Mo, Y. S. Liu, and Z. C. Hu (2011), Zircon U–Pb geochronology and Hf isotopes of the Early Cretaceous Rena Co rhyolites from southern margin of Qiangtang, Tibet, and their implications, *Acta Petrol. Sin.*, *27*, 2034–2044.

Chauvel, C., E. Lewin, M. Carpentier, N. T. Arndt, and J. C. Marini (2008), Role of recycled oceanic basalt and sediment in generating the Hf–Nd mantle array, *Nat. Geosci.*, *1*, 64–67.

Chen, L., Z.-F. Zhao, and Y.-F. Zheng (2014), Origin of andesitic rocks: Geochemical constraints from Mesozoic volcanics in the Luzong basin, South China, *Lithos*, *190–191*, 220–239.

Chung, S.-L., M.-F. Chu, Y. Q. Zhang, Y. W. Xie, C.-H. Lo, T.-Y. Lee, C.-Y. Lan, X. H. Li, Q. Zhang, and Y. Z. Wang (2005), Tibetan tectonic evolution inferred from spatial and temporal variations in post-collisional magmatism, *Earth Sci. Rev.*, *68*, 173–196.

Class, C., D. M. Miller, S. L. Goldstein, and C. H. Langmuir (2000), Distinguishing melt and fluid subduction components in Umnak Volcanics, Aleutian Arc, *Geochem. Geophys. Geosyst. 1*, 1004.

Dhuime, B., A. Wuestefeld, and C. J. Hawkesworth (2015), Emergence of modern continental crust about 3 billion years ago, *Nat. Geosci.*, *8*, 552–555.

Eiler, J. M. (2001), Oxygen isotope variations in basaltic lavas and upper mantle rocks, *Rev. Mineral. Geochem.*, *43*, 319–364.

Elliott, T., T. Plank, A. Zindler, W. White, and B. Bourdon (1997), Element transport from slab to volcanic front in the Mariana arc, *J. Geophys. Res.*, *102*, 14,991–15,019.

Fan, J.-J., C. Li, C.-M. Xie, and M. Wang (2014), Petrology, geochemistry, and geochronology of the Zhonggang ocean island, northern Tibet: Implications for the evolution of the Banggongco–Nujiang oceanic arm of the Neo-Tethys, *Int. Geol. Rev.*, *56*, 1504–1520.

Fan, J.-J., C. Li, C.-M. Xie, M. Wang, and J.-W. Chen (2015), Petrology and U–Pb zircon geochronology of bimodal volcanic rocks from the Maierze Group, northern Tibet: Constraints on the timing of closure of the Banggong–Nujiang Ocean, *Lithos*, *227*, 148–160.

Gerya, T. V., and D. A. Yuen (2003), Rayleigh-Taylor instabilities from hydration and melting propel 'cold plumes' at subduction zones, *Earth Planet. Sci. Lett*, *212*, 47–62.

Gerya, T. V., D. A. Yuen, and E. O. D. Sevre (2004), Dynamical causes for incipient magma chambers above slabs, *Geology*, *32*, 89–92.

Guo, Z., M. Wilson, L. Zhang, M. Zhang, Z. Cheng, and J. Liu (2014), The role of subduction channel mélanges and convergent subduction systems in the petrogenesis of post-collisional K-rich mafic magmatism in NW Tibet, *Lithos*, *198*, 184–201.

Guo, Z. F., M. Wilson, M. L. Zhang, Z. H. Cheng, and L. H. Zhang (2013), Post-collisional, K-rich mafic magmatism in south Tibet: Constraints on Indian slab-to-wedge transport processes and plateau uplift, *Contrib. Mineral. Petrol.*, *165*, 1311–1340.

Guynn, J., P. Tropper, P. Kapp, and G. E. Gehrels (2013), Metamorphism of the Amdo metamorphic complex, Tibet: Implications for the Jurassic tectonic evolution of the Bangong suture zone, *J. Metamorph. Geol.*, *31*, 705–727.

Guynn, J. H., P. Kapp, A. Pullen, M. Heizler, G. Gehrels, and L. Ding (2006), Tibetan basement rocks near Amdo reveal "missing" Mesozoic tectonism along the Bangong suture, central Tibet, *Geology*, *34*, 505–508.

Hacker, B. R., P. B. Kelemen, and M. D. Behn (2011), Differentiation of the continental crust by relamination, *Earth. Planet. Sci. Lett.*, *307*, 501–516.

Hao, L.-L., Q. Wang, D. A. Wyman, Q. Ou, W. Dan, Z.-Q. Jiang, F.-Y. Wu, J.-H. Yang, X.-P. Long, and J. Li (2016), Underplating of basaltic magmas and crustal growth in a continental arc: Evidence from Late Mesozoic intermediate–felsic intrusive rocks in southern Qiangtang, central Tibet, *Lithos*, *245*, 223–242.

Harrison, T. M., P. Copeland, W. S. F. Kidd, and A. Yin (1992), Raising tibet, *Science*, *255*, 1663–1670.

Hildreth, W., and S. Moorbath (1988), Crustal contributions to arc magmatism in the Andes of central Chile, *Contrib. Mineral. Petrol.*, *98*, 455–489.

Hofmann, A. W. (1988), Chemical differentiation of the Earth: The relationship between mantle, continental crust, and oceanic crust, *Earth. Planet. Sci. Lett.*, *90*, 297–314.

Johnson, M. C., and T. Plank (1999), Dehydration and melting experiments constrain the fate of subducted sediments, *Geochem. Geophys. Geosyst. 1*, 1007.

Kapp, P., M. A. Murphy, A. Yin, T. M. Harrison, L. Ding, and J. R. Guo (2003), Mesozoic and Cenozoic tectonic evolution of the Shiquanhe area of western Tibet, *Tectonics 22*(4), 1029, doi:10.1029/2001TC001332.

Kapp, P., A. Yin, T. M. Harrison, and L. Ding (2005), Cretaceous-Tertiary shortening, basin development, and volcanism in central Tibet, *Geol. Soc. Am. Bull.*, *117*(7–8), 865–878.

Kelemen, P. B. (1995), Genesis of high Mg# andesites and the continental crust, *Contrib. Mineral. Petrol.*, *120*, 1–19.

Li, C., Q. G. Zhai, Y. S. Dong, and X. P. Huang (2006), Discovery of eclogite and its geological significance in Qiangtang area, central Tibet, *Chin. Sci. Bull.*, *51*, 1095–1100.
Li, J., K. Qin, G. Li, B. Xiao, J. Zhao, and L. Chen (2011), Magmatic-hydrothermal evolution of the Cretaceous Duolong gold-rich porphyry copper deposit in the Bangongco metallogenic belt, Tibet: Evidence from U-Pb and 40Ar/39Ar geochronology, *J. Asian. Earth. Sci.*, *41*, 525–536.
Li, J. X., G. M. Li, K. Z. Qin, and B. Xiao (2008), Geochemistry of porphyries and volcanic rocks and ore-forming geochronology of Duobuza gold-rich porphyry copper deposit in Bangonghu belt, Tibet: Constrain on metallogenic tectonic settings, *Acta. Petrol. Sin.*, *24*(3), 531–543.
Li, J. X., K.-Z. Qin, G.-M. Li, B. Xiao, J.-X. Zhao, M.-J. Cao, and L. Chen (2013), Petrogenesis of ore-bearing porphyries from the Duolong porphyry Cu–Au deposit, central Tibet: Evidence from U–Pb geochronology, petrochemistry and Sr–Nd–Hf–O isotope characteristics, *Lithos*, *160-161*, 216–227.
Li, J. X., K.-Z. Qin, G.-M. Li, J. P. Richards, J.-X. Zhao, and M.-J. Cao, (2014), Geochronology, geochemistry, and zircon Hf isotopic compositions of Mesozoic intermediate–felsic intrusions in central Tibet: Petrogenetic and tectonic implications, *Lithos*, *198-199*, 77–91.
Li, S.-M., D.-C. Zhu, Q. Wang, Z.-D. Zhao, Q.-L. Sui, S.-A. Liu, D. Liu, and X.-X. Mo (2014), Northward subduction of Bangong–Nujiang Tethys: Insight from Late Jurassic intrusive rocks from Bangong Tso in western Tibet, *Lithos*, *205*, 284–297.
Liu, D., Q. S. Huang, S. Q. Fan, L. Y. Zhang, R. D. Shi, and L. Ding (2014), Subduction of the Bangong–Nujiang Ocean: Constraints from granites in the Bangong Co area, Tibet, *Geol. J.*, *49*, 188–206.
Liu, D., R. Shi, L. Ding, Q. Huang, X. Zhang, Y. Yue, and L. Zhang (2015), Zircon U–Pb age and Hf isotopic compositions of Mesozoic granitoids in southern Qiangtang, Tibet: Implications for the subduction of the Bangong–Nujiang Tethyan Ocean, *Gondwana Res.*, doi: 10.1016/j.gr.2015.04.007, in press.
Liu, S., R. Z. Hu, S. Gao, C. X. Feng, I. M. Coulson, G. Y. Feng, Y. Q. Qi, Y. H. Yang, C. G. Yang, and L. Tang (2012), U–Pb zircon age, geochemical and Sr–Nd isotopic data as constraints on the petrogenesis and emplacement time of andesites from Gerze, southern Qiangtang Block, northern Tibet, *J. Asian. Earth Sci.*, *45*, 150–161.
Ma, L., Q. Wang, Z.-X. Li, D. A. Wyman, Z.-Q. Jiang, J.-H. Yang, G.-N. Gou, and H.-F. Guo (2013), Early Late Cretaceous (ca. 93Ma) norites and hornblendites in the Milin area, eastern Gangdese: Lithosphere–asthenosphere interaction during slab roll-back and an insight into early Late Cretaceous (ca. 100–80Ma) magmatic "flare-up" in southern Lhasa (Tibet), *Lithos*, *172-173*, 17–30.
Marschall, H. R., and J. C. Schumacher (2012), Arc magmas sourced from melange diapirs in subduction zones, *Nat. Geosci.*, *5*, 862–867.
McKenzie, D., and R. K. O'Nions (1991), Partial melt distributions from inversion of rare earth element concentrations, *J. Petrol.*, *32*, 1021–1091.
Middlemost, E. A. K. (1994), Naming materials in the magma/igneous rock system, *Earth. Sci. Rev.*, *37*, 215–224.
Plank, T., and C. H. Langmuir (1998), The chemical composition of subducting sediment and its consequences for the crust and mantle, *Chem. Geol.*, *145*, 325–394.
Qu, X. M., and H. B. Xin (2006), Ages and tectonic environment of the Bangong Co porphyry copper belt in western Tibet, China, *Geol. Bull. China*, *25*(7), 792–799.
Rapp R. P., and E. B. Watson (1995), Dehydration melting of metabasalt at 8–32 kbar: Implications for continental growth and crust-mantle recycling, *J. Petrol.*, *36*, 891–931.
Rudnick R. L., and S. Gao (2003), Composition of the continental crust, in *Treatise on Geochemistry*, vol. 3, edited by H. D. Holland and K. K. Turekian, pp. 1–64, Elsevier, Amsterdam, Netherlands.
Rudnick, R. L. (1995), Making continental crust, *Nature*, *378*, 571–577.
Sun, S. S., and W. F. McDonough (1989), Chemical and isotopic systematics of oceanic basalts: Implications for mantle composition and processes, *Geol. Soc. Spec. Publ.*, *42*, 313–345.
Tang, G.-J., Q. Wang, D. A. Wyman, Z.-X. Li, Y.-G. Xu, and Z.-H. Zhao (2012), Metasomatized lithosphere–asthenosphere interaction during slab roll-back: Evidence from Late Carboniferous gabbros in the Luotuogou area, Central Tianshan, *Lithos*, *155*, 67–80.
Taylor, S. R. (1967), The origin and growth of continents, *Tectonophysics*, *4*, 17–34.
Taylor, S. R., and S. M. McLennan (1985), *The Continental Crust: Its Composition and Evolution*, Blackwell, Melbourne.
Taylor, W. (1998), An experimental test of some geothermometer and geobarometer formulations for uppermantle peridotites with application to the thermobarometry of fertile lherzolite and garnet websterite, *Neues Jahrb. Mineral. Abh.*, *172*, 381–408.
Valley, J. W., P. D. Kinny, D. J. Schulze, and M. J. Spicuzza (1998), Zircon megacrysts from kimberlite: Oxygen isotope variability among mantle melts, *Contrib. Mineral. Petrol.*, *133*, 1–11.
von Huene, R., and D. W. Scholl (1991), Observations at convergent margins concerning sediment subduction, subduction erosion, and the growth of continental crust, *Rev. Geophys.*, *29*, 279–316.
Wang, B. D., L. Q. Wang, S. L. Chung, J. L. Chen, F. G. Yin, H. Liu, X. B. Li, and L. K. Chen (2016), Evolution of the Bangong–Nujiang Tethyan ocean: Insights from the geochronology and geochemistry of mafic rocks within ophiolite, *Lithos*, *245*, 18–33.
Wang, Q., J. F. Xu, P. Jian, Z. W. Bao, Z. H. Zhao, C. F. Li, X. L. Xiong, and J. L. Ma (2006), Petrogenesis of adakitic porphyries in an extensional tectonic setting, Dexing, South China: Implications for the genesis of porphyry copper mineralization, *J. Petrol.*, *47*, 119–144.
Xu, M. J., C. Li, X. Z. Zhang, and Y. W. Wu (2014), Nature and evolution of the Neo-Tethys in central Tibet: Synthesis of ophiolitic petrology, geochemistry, and geochronology, *Int. Geol. Rev.*, *56*, 1072–1096.
Xu, Y.-G., J.-L. Ma, X.-L. Huang, Y. Iizuka, S.-L. Chung, Y.-B. Wang, and X.-Y. Wu (2004), Early Cretaceous gabbroic complex from Yinan, Shandong Province: Petrogenesis and mantle domains beneath the North China Craton, *Int. J. Earth Sci. (Geol. Rundsch.)*, *93*, 1025–1041.
Yin, A., and T. M. Harrison (2000), Geologic evolution of the Himalayan-Tibetan orogen, *Annu. Rev. Earth. Planet. Sci.*, *28*, 211–280.
Zhang, K. J., Y. X. Zhang, X. C. Tang, and B. Xia (2012), Late Mesozoic tectonic evolution and growth of the Tibetan plateau prior to the Indo-Asian collisionCentral Tibetan Meso-Tethyan oceanic plateau, *Earth Sci. Rev.*, *114*, 236–249.
Zhang, K. J., B. Xia, Y. X. Zhang, W. L. Liu, L. Zeng, J. F. Li, and L. F. Xu (2014), Central Tibetan Meso-Tethyan oceanic plateau, *Lithos*, *210*, 278–288.
Zhang, X. R., R. D. Shi, Q. S. Huang, D. L. Liu, X. H. Gong, S. S. Chen, K. Wu, G. D. Yi, Y. L. Sun, and L. Ding (2014), Early Jurassic high-pressure metamorphism of the Amdo terrane, Tibet: Constraints from zircon U-Pb geochronology of mafic granulites, *Gondwana Res.*, *26*, 975–985.
Zhao, Z.-F., L.-Q. Dai, and Y.-F. Zheng (2013), Postcollisional mafic igneous rocks record crust-mantle interaction during continental deep subduction, *Sci. Rep.*, *3*, 3413, doi:10.1038/srep03413.
Zheng, Y.-F. (2012), Metamorphic chemical geodynamics in continental subduction zones, *Chem. Geol.*, *328*, 5–48.
Zheng, Y.-F., Y. Chen, L. Dai, and Z. Zhao (2015), Developing plate tectonics theory from oceanic subduction zones to collisional orogens, *Sci. China. Ser. D. 58*, 1045–1069.

Zhu, D. C., G. Pan, X. Mo, L. Wang, Z. Zhao, Z. Liao, Q. Geng, and G. Dong (2006), Identification for the Mesozoic OIB-type basalts in central Qinghai-Tibetan Plateau: Geochronology, geochemistry and their tectonic setting, *Acta. Geol. Sin.*, *80*, 1312–1328.

Zhu, D. C., Z. D. Zhao, Y. L. Niu, X. X. Mo, S. L. Chung, Z. Q. Hou, L. Q. Wang, and F. Y. Wu (2011), The Lhasa Terrane: Record of a microcontinent and its histories of drift and growth, *Earth. Planet. Sci. Lett.*, *301*, 241–255.

Zhu, D.-C., S.-M. Li, P. A. Cawood, Q. Wang, Z.-D. Zhao, S.-A. Liu, and L.-Q. Wang (2016), Assembly of the Lhasa and Qiangtang terranes in central Tibet by divergent double subduction, *Lithos*, *245*, 7–17.